Synapse-specific and size-dependent mechanisms of spine structural plasticity accompanying synaptic weakening

Won Chan Oh, Travis C. Hill, and Karen Zito[1]

Center for Neuroscience, University of California, Davis, CA 95616

Edited by Michael Eldon Greenberg, Harvard Medical School, Boston, MA, and approved November 28, 2012 (received for review August 23, 2012)

Refinement of neural circuits in the mammalian cerebral cortex shapes brain function during development and in the adult. However, the signaling mechanisms underlying the synapse-specific shrinkage and loss of spiny synapses when neural circuits are remodeled remain poorly defined. Here, we show that low-frequency glutamatergic activity at individual dendritic spines leads to synapse-specific synaptic weakening and spine shrinkage on CA1 neurons in the hippocampus. We found that shrinkage of individual spines in response to low-frequency glutamate uncaging is saturable, reversible, and requires NMDA receptor activation. Notably, shrinkage of large spines additionally requires signaling through metabotropic glutamate receptors (mGluRs) and inositol 1,4,5-trisphosphate receptors (IP_3Rs), supported by higher levels of mGluR signaling activity in large spines. Our results support a model in which signaling through both NMDA receptors and mGluRs is required to drive activity-dependent synaptic weakening and spine shrinkage at large, mature dendritic spines when neural circuits undergo experience-dependent modification.

two-photon microscopy | long-term depression | synaptic plasticity | spine dynamics

Structural plasticity of neurons, such as the growth and retraction of dendritic spines, is thought to contribute to the experience-dependent changes in brain circuitry that mediate learning and memory (1, 2). In particular, the destabilization and loss of spiny synapses plays a critical role in the refinement of neural circuits during development and during learning. Indeed, spine elimination occurs more frequently than does spine formation in young rodents between the first and the third month of age (3–5), a period when experience-dependent refinement of neural circuitry is in its peak. Furthermore, several in vivo studies demonstrate that manipulations leading to experience-dependent circuit plasticity also increase the rate of spine shrinkage and loss (6–9). However, it remains unclear how neural activity drives the selective shrinkage and loss of individual dendritic spines in response to sensory experience.

Dendritic spines occur in a wide variety of shapes and sizes (10, 11), and their stability is strongly correlated with spine size (3, 12, 13). Small spines are in general more motile and thought to serve as substrates for plasticity, or "learning" spines; large spines are more stable and thought to serve as components of functioning neural circuits, or "memory" spines (12, 14). It is the selective shrinkage and loss of individual circuit-incorporated, persistent spines that underlies experience-dependent circuit refinement (6, 9, 15). Thus, experience-dependent circuit remodeling requires an activity-dependent mechanism that selectively induces shrinkage and retraction of those specific individual dendritic spines that are no longer useful for circuit function.

Previous studies have established that low-frequency glutamatergic stimulation (LFS), which causes long-term depression (LTD) of synaptic transmission in the hippocampus (16), also leads to dendritic spine shrinkage and retraction (17–20). In these studies, however, LTD was induced using local electrical stimulation at multiple, unidentified synapses simultaneously and resulted in shrinkage and retraction of a population of dendritic spines, leaving the mechanisms underlying the induction of synapse-specific spine shrinkage unresolved. In contrast, the input-specificity of spine enlargement associated with long-term potentiation (LTP) has been established for almost a decade (21), leading to speculation that spine shrinkage simply may not occur via an input-specific mechanism. Instead, shrinkage and retraction of individual dendritic spines could be initiated as a result of cooperation among or competition between neighboring spines.

Here we use two-photon glutamate uncaging, time-lapse imaging, and whole-cell recordings to address the mechanisms by which neural activity drives the shrinkage and loss of individual dendritic spines. We show that prolonged, low-frequency glutamate uncaging at individual spines on hippocampal CA1 pyramidal neurons leads to input-specific and long-lasting synaptic weakening and spine shrinkage. NMDA receptors are upstream regulators of activity-dependent shrinkage for all spines. Intriguingly, we found that shrinkage of individual large spines additionally requires group I metabotropic glutamate receptor (mGluR) and inositol 1,4,5-trisphosphate receptor (IP_3R) activation, which is supported by more extensive group I mGluR signaling activity in large spines. Our data support a model in which low-frequency neural activity at individual dendritic spines selectively drives weakening and shrinkage of spine synapses by input-specific and size-dependent mechanisms.

Results

Low-Frequency Uncaging Induces Synapse-Specific LTD and Spine Shrinkage. To identify glutamatergic activity patterns that lead to synapse-specific LTD, focal photolysis of 4-methoxy-7-nitroindolinyl (MNI)-caged glutamate (22) was used to stimulate individual dendritic spines. We rationally designed an uncaging paradigm to induce synapse-specific LTD (*SI Materials and Methods*). In brief, we adjusted established protocols that induce LTP at individual dendritic spines (21) to reduce the magnitude and prolong the duration of calcium influx according to the Bienenstock, Cooper, and Munro (BCM) model (23). Our low-frequency uncaging (LFU) stimulus consisted of 90 pulses at 0.1 Hz paired with depolarization to 0 mV (Fig. 1*A*). Uncaging-evoked postsynaptic currents (uEPSCs) were recorded from one target spine and one or two neighboring spines at 5-min intervals before and after LFU at the target spine. LFU at individual spines successfully induced depression of uEPSCs that lasted at least 30 min after the start of uncaging ($P < 0.01$; Fig. 1 *B* and *C*). Importantly, uEPSCs of unstimulated neighboring spines did not show any de-

Author contributions: W.C.O. and K.Z. designed research; W.C.O. performed research; T.C.H. contributed new reagents/analytic tools; W.C.O. analyzed data; and W.C.O. and K.Z. wrote the paper.

The authors declare no conflict of interest.

This article is a PNAS Direct Submission.

[1]To whom correspondence should be addressed. E-mail: kzito@ucdavis.edu.

See Author Summary on page 1154 (volume 110, number 4).

This article contains supporting information online at www.pnas.org/lookup/suppl/doi:10.1073/pnas.1214705110/-/DCSupplemental.

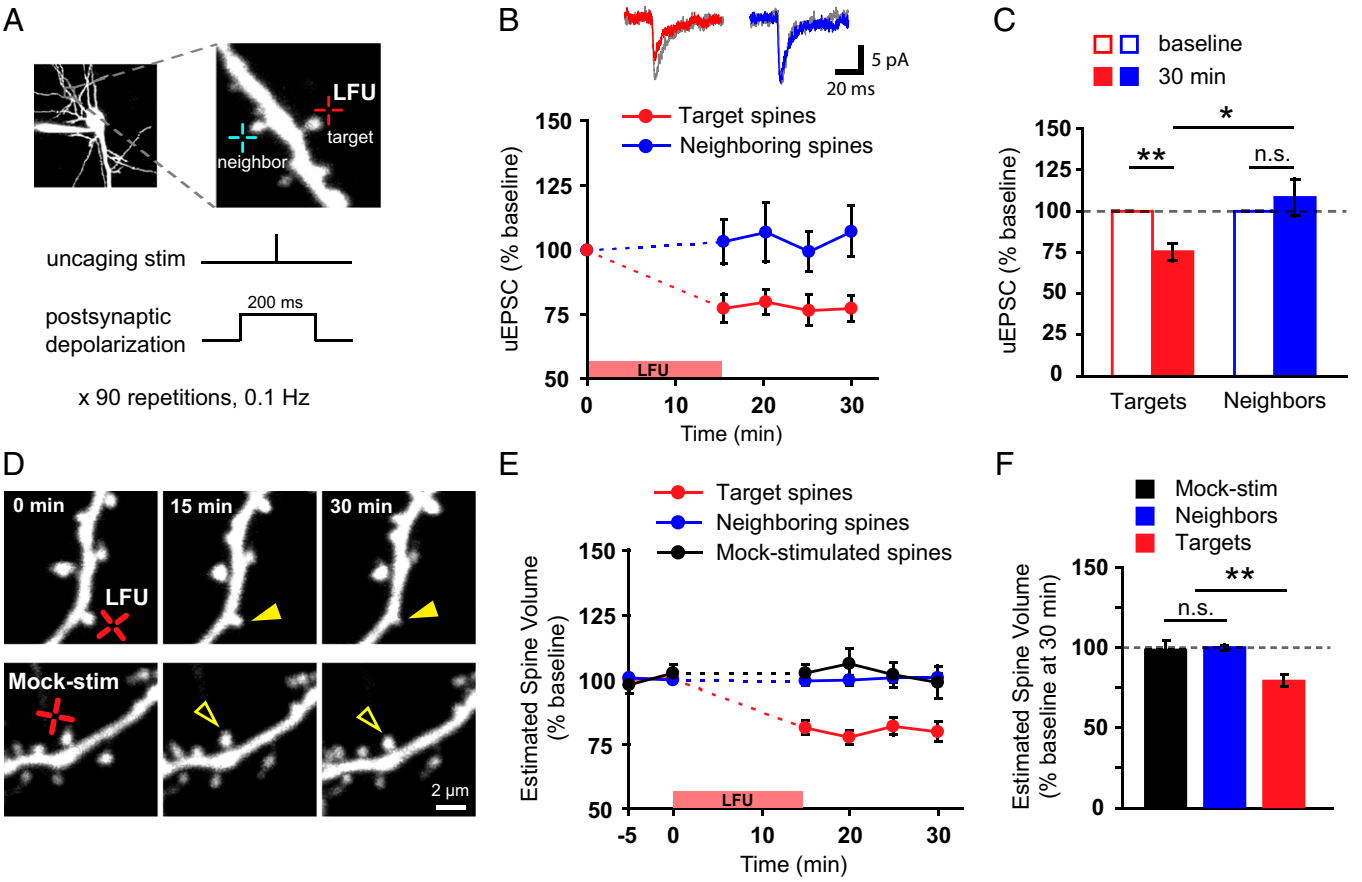

Fig. 1. LFU at individual dendritic spines leads to synapse-specific LTD and spine shrinkage. (*A*) A target spine (red cross) was stimulated with LFU (90 pulses at 0.1 Hz) while the cell was stepped from −65 to 0 mV. Neighboring unstimulated spines (blue cross) served as controls. (*B*) LFU decreased the uEPSC amplitude of target spines (red circles; $n = 15$ spines, 15 cells) compared with unstimulated neighboring spines (blue circles; $P < 0.05$ at all post-LFU time points; $n = 16$ spines). (*Inset*) Representative uEPSC traces (average of 8–10 trials) during baseline (gray) and 30 min after LFU (target in red; neighbor in blue). (*C*) uEPSC amplitude of the target spines (red bar) was significantly decreased 30 min after the start of LFU compared with baseline (open red bar) and also to neighboring spines (blue bar). Neighboring spines were not depressed compared with baseline (open blue bar; $P = 0.47$). (*D*) Images of dendrites from EGFP-transfected CA1 neurons. A target spine exposed to LFU (*Upper*) in nominal Mg^{2+} shrank (yellow arrowheads); a mock-stimulated spine (*Lower*) did not (open yellow arrowheads). (*E*) LFU decreased the volume of target spines compared with baseline (red circles; $P < 0.01$ at all post-LFU time points; $n = 42$ spines, 42 cells). In contrast, the volume of neighboring spines (blue circles; $n = 230$ spines) and mock-stimulated spines (black circles; $n = 18$ spines, 18 cells) did not decrease. (*F*) LFU significantly decreased the size of target spines (red bar) relative to neighboring spines (blue bar) and mock-stimulated spines (black bar) at 30 min. *$P < 0.05$; **$P < 0.01$. Error bars are SEM; n.s., not significant.

crease in amplitude ($P = 0.47$; Fig. 1 *B* and *C*). These results demonstrate that depolarization alone did not induce any functional plasticity and that LFU-induced depression is synapse-specific.

Shrinkage of dendritic spines has been associated with LTD (18). However, in these studies, the association between physiological and morphological plasticity could not be resolved at the single-spine level; because many synapses were stimulated simultaneously, it could not be determined whether spine shrinkage occurred only at stimulated synapses in an input-specific manner. Therefore, to address whether spine shrinkage is tightly coupled to synaptic depression at the level of single spines, we used time-lapse imaging to examine the effect of LFU on the volume of stimulated target spines and unstimulated neighboring spines (Fig. 1*D*). We found that LFU led to a significant and stable decrease in the size of target spines ($P < 0.01$) but not of neighboring spines ($P = 0.78$; Fig. 1 *D*–*F*). In addition, spines that were exposed to a mock-LFU stimulus (identical conditions except without MNI-glutamate) did not decrease in size ($P = 0.85$; Fig. 1 *D*–*F*). Together, these results demonstrate that LFU not only leads to synapse-specific LTD but also induces shrinkage of individual spines in an input- and synapse-specific manner.

LFU-Induced Spine Shrinkage Is Long-Lasting, Saturable, and Reversible. When targeted toward entire dendritic segments, LTD-inducing synaptic stimulation can lead to both spine shrinkage and elimination of a population of spines (17, 18). To address whether LFU-induced spine shrinkage at individual dendritic spines is long-lasting and eventually leads to spine elimination, we performed extended time-lapse imaging up to 60 min after LFU stimulation (Fig. 2*A*, *Top*). We found that LFU caused a stable, long-lasting (>60 min) decrease in spine size ($P < 0.01$) rather than complete spine elimination (Fig. 2 *B* and *C*), suggesting that a single episode of LFU at an individual spine is not sufficient to trigger complete spine loss within this time period. Notably, individual spines shrank to varying extents in response to LFU; however, there was no discernable subgroup of spines that were resistant to LFU-induced shrinkage (Fig. S1). We next tested whether repeated LFU could induce spine elimination (Fig. 2*A*, *Middle*). Again, we found that double LFU led to a stable spine shrinkage ($P < 0.05$), indicating that the additional LFU stimulus was ineffective at inducing further shrinkage (Fig. 2 *B* and *C*). Mock-stimulated spines (Fig. 2*A*, *Bottom*) were also examined and did not show any significant changes in size during 60 min of imaging session ($P > 0.3$ at all post-LFU time points; Fig. 2 *B* and *C*). Thus, LFS of individual dendritic spines causes long-lasting and saturable spine shrinkage.

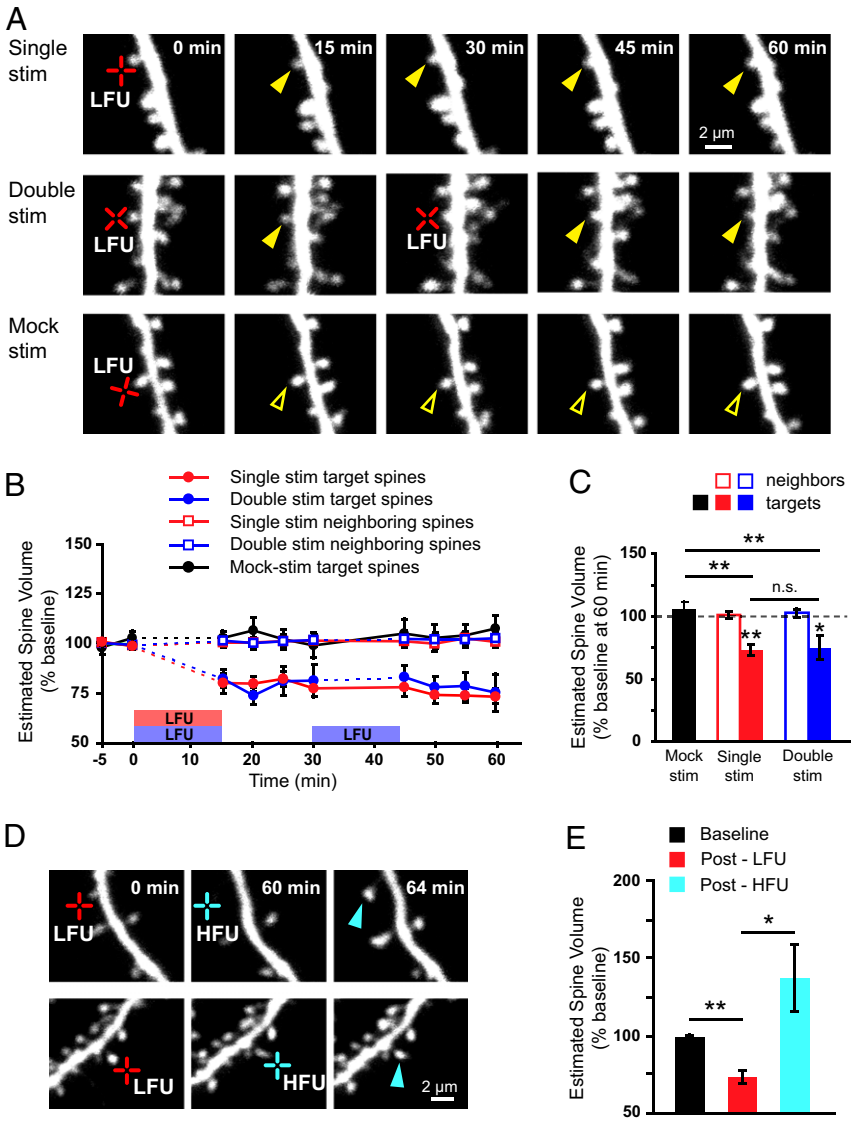

Fig. 2. LFU-induced spine shrinkage is long-lasting, saturable, and reversible. (*A*) A reduction in spine size was observed in response to single LFU (yellow arrowheads, *Top*) or double LFU (yellow arrowheads, *Middle*). In contrast, a mock-stimulated spine did not shrink in response to single LFU (open yellow arrowheads, *Bottom*). (*B*) Target spines persistently decreased in size in response to single LFU (red circles; $n = 21$ spines, 21 cells) or double LFU (blue circles; $n = 15$ spines, 15 cells) compared with baseline. The size decrease of double-stimulated target spines was indistinguishable from that of single-stimulated spines ($P > 0.31$ at all post-LFU time points). Neighboring spines (open red squares, $n = 132$ spines; open blue squares, $n = 80$ spines) and mock-stimulated spines (black circles; $n = 18$ spines, 18 cells) did not shrink. Data from Fig. 1*E* are included in this graph. (*C*) Single LFU (red bar) and double LFU (blue bar) significantly decreased the size of target spines relative to neighboring spines (open red or blue bar, respectively) and mock-stimulated spines (black bar) at 60 min. The decrease in target spine size in response to single LFU was indistinguishable from that from double LFU ($P = 0.85$) at 60 min. (*D*) Images of dendritic spines exposed to LFU (red cross) followed by HFU (200 pulses of 1-ms duration at 10 Hz; light blue cross). LFU-induced spine shrinkage was reversed in response to HFU (light blue arrowheads). (*E*) Shrinkage of target spines exposed to LFU (red bar) relative to baseline (black bar) was reversed after HFU (light blue bar; $n = 16$ spines, 16 cells). $^*P < 0.05$; $^{**}P < 0.01$. Error bars are SEM; n.s., not significant.

To confirm that LFU-induced spine shrinkage does not reflect excitotoxicity, we examined whether shrunk spines were functionally intact and still able to undergo repotentiation at the end of the imaging session. To this end, LFU-induced destabilized target spines were stimulated with a high-frequency glutamate uncaging protocol (HFU, 200 pulses at 10 Hz). As expected, LFU-induced shrunk spines were significantly enlarged after the HFU stimulus ($P < 0.05$; Fig. 2 *D* and *E*), demonstrating that spine shrinkage was reversible and not due to deterioration of individual spines. Our data demonstrate that individual spines can undergo bidirectional structural modifications such as decrease and increase in size, depending on the activity patterns they receive.

Activity-Dependent Shrinkage of Individual Spines Requires NMDAR Activation. What signaling mechanisms drive synapse-specific spine shrinkage? NMDA receptor (NMDAR) inhibition significantly decreases spine elimination rates both in vitro (13) and in vivo (15). In addition, NMDAR activation is required for LFS-induced spine shrinkage and retraction (17, 18). Thus, we examined whether input- and synapse-specific, LFU-induced spine shrinkage also depends on NMDAR activation (Fig. 3*A*). Indeed, we found that pharmacological blockade of NMDAR with (RS)-3-(2-carboxypiperazin-4-yl)-propyl-1-phosphonic acid (CPP) (10 μM) completely prevented LFU-induced spine shrinkage ($P = 0.45$; Fig. 3 *B* and *C*). Bath application of CPP did not influence spine morphology by itself because unstimulated neighboring spines did not show any significant change in size (Fig. 3 *A*–*C*). This result demonstrates that NMDAR activation is necessary for LFU-induced spine shrinkage.

In addition to NMDAR, involvement of mGluR signaling pathway in the regulation of spine morphology is suggested by the fact that stimulation of group I mGluRs by (RS)-3,5-dihydroxyphenylglycine (DHPG) (group I mGluR agonist) causes morphological changes in dendritic spines, with a shift toward a thinner and immature morphology (24). We therefore examined the role of mGluRs in activity-dependent spine shrinkage using a competitive antagonist of mGluRs [(RS)-alpha-methyl-4-carboxyphenylglycine (MCPG), 0.25 mM] (Fig. 3*A*). Interestingly, we found that blocking mGluRs using bath-applied MCPG resulted in a partial inhibition of LFU-induced spine shrinkage ($P = 0.19$) without affecting neighboring unstimulated spines (Fig. 3 *B* and *C*). This partial inhibition was not due to lack of efficacy of MCPG on mGluRs (Fig. S2). These results support that activation of intracellular pathways by group I mGluRs could also play some role in triggering spine shrinkage.

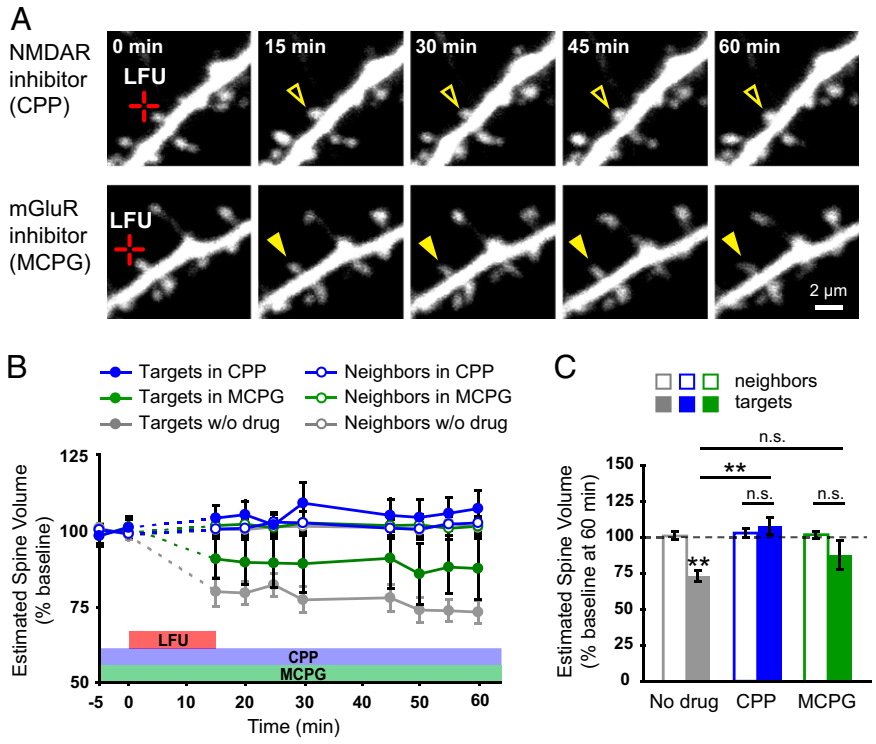

Fig. 3. Activity-dependent spine shrinkage requires NMDAR activation. (*A*) LFU-induced spine shrinkage was blocked in the presence of CPP (open yellow arrowheads) but not in the presence of MCPG (yellow arrowheads). (*B*) Target spine shrinkage in response to LFU was completely blocked in the presence of CPP (blue circles; $P > 0.19$ at all post-LFU time points; $n = 21$ spines, 21 cells) and partially, but nonsignificantly, blocked in the presence of MCPG (green circles; $P > 0.18$ at all post-LFU time points; $n = 18$ spines, 18 cells). Data without drug (gray circles) are from Fig. 2. (*C*) In the presence of CPP, the volume of stimulated target spines (blue bar; $n = 21$ spines) at 60 min after LFU was indistinguishable ($P = 0.45$) from that of unstimulated neighbors (open blue bar; $n = 143$ spines). In the presence of MCPG, the volume of stimulated target spines (green bar; $n = 18$ spines) at 60 min after LFU showed a nonsignificant trend ($P = 0.19$) toward decreasing relative to that of unstimulated neighbors (open green bar; $n = 108$ spines). The volume of control spines without drug (gray bar; $n = 21$ spines) at 60 min was significantly smaller compared with that of target spines in CPP (blue bar) but not to that in MCPG (green bar; $P = 0.20$). Data without drug (gray bars) are from Fig. 2. $^{**}P < 0.01$. Error bars are SEM; n.s., not significant.

Group I mGluR Activation Is Required for Shrinkage of Large Spines. We wondered whether the partial inhibition of spine shrinkage by MCPG might reflect a heterogeneous population of spines that included subpopulations with different mGluR-dependency for shrinkage. Indeed, recent work demonstrated that only the largest endoplasmic reticulum-containing spines can undergo long-term synaptic depression mediated exclusively by mGluR activation (25). Therefore, we examined whether activity-dependent shrinkage of large spines was more sensitive to mGluR antagonists than that of small spines. Spines were categorized into two groups according to their relative size compared with other spines on the same dendritic segment: "small" (relative size < mean) vs. "large" (relative size > mean). Remarkably, we found that inhibition of mGluR activation with MCPG completely blocked ($P = 0.48$) LFU-induced shrinkage of large spines, even though small spine shrinkage was unaffected ($P < 0.05$; Fig. 4 *A–C*). We further examined the role of group I mGluRs (mGluR1 and mGluR5) using group I-specific antagonists, 7-(hydroxyimino)cyclopropa [b]chromen-1a-carboxylate ethyl ester (CPCCOEt, 45 μM) and 2-methyl-6-(phenylethynyl)pyridine hydrochloride (MPEP, 15 μM). Consistent with results using MCPG, group I mGluR antagonists completely blocked ($P = 0.79$) LFU-induced destabilization of large, but not small, spines ($P < 0.05$; Fig. 4 *A–C*). In contrast, NMDAR inhibition completely abolished spine shrinkage for both groups (Fig. S3). Thus, our data demonstrate that activity-dependent shrinkage of large spines requires both NMDAR and group I mGluR activation.

The role of group I mGluRs in LFU-induced large spine shrinkage raised an exciting question about the extent of mGluR signaling activity in different sizes of spines. To examine mGluR activity in individual spines, we used an electrophysiological readout of group I mGluR activation (26): reduced amplitude of AMPA receptor (AMPAR)-uEPSCs after DHPG application (Fig. 4*D*). Consistent with other DHPG-induced mGluR-LTD studies (27), we found that 5 min wash-in of 100 μM DHPG rapidly induced depression of the AMPAR-uEPSCs at the single-spine level ($P < 0.01$). Moreover, analysis of the uEPSCs from different sizes of spines revealed that only large spines exhibited a significant decrease in the magnitude of AMPAR-uEPSCs ($P < 0.01$; Fig. 4 *D* and *E*), demonstrating that large spines undergo greater group I mGluR-mediated synaptic depression in response to DHPG than small spines. Importantly, LFU (Fig. 1 *A–C*) significantly decreased the uEPSC amplitudes of both large and small spines (Fig. S4), indicating that the lack of effect of DHPG on small spines was not due to technical limitation of detecting decreases in small uEPSCs. Thus, we propose that group I mGluR signaling plays an essential role in modulating the structure and function of large synapses during activity-dependent plasticity.

Activity-Dependent Large Spine Shrinkage Requires IP_3R Activation. What signaling mechanisms act downstream of the mGluRs to shrink large spines? Glutamate binding to group I mGluRs leads to activation of phospholipase Cβ (PLCβ) (28). When activated, PLCβ leads to activation of PKC due to the production of diacylglycerol. Myristoylated alanine-rich C-kinase substrate (MARCKS), a substrate of PKC, plays a role in maintaining the stability and shape of dendritic spines in mature neurons (29). To test a possible role for PKC activity in activity-dependent large spine shrinkage, we investigated whether GF109203X (1 μM), an inhibitor of PKC, blocked the large spine shrinkage induced by LFU stimulus (Fig. 5*A*). Bath-application of GF109203X at least 15 min before LFU stimulation did not prevent LFU-induced shrinkage of large spines ($P < 0.01$; Fig. 5 *B* and *C*). The effectiveness of GF109203X as a PKC inhibitor was verified electrophysiologically in our hippocampal culture system (Fig. S5). We therefore conclude that PKC is not involved in LFU-induced large spine shrinkage.

Activation of PLCβ also generates IP_3, which stimulates calcium release from intracellular stores (28). It has been shown that large mushroom-shaped spines are more likely to contain endoplasmic reticulum (10), which could contribute to calcium signaling during structural plasticity. We therefore investigated the role of calcium release from intracellular stores in the activity-dependent large spine shrinkage. We found that LFU-induced shrinkage of large spines was completely abolished in the presence of bath-applied Xestospongin C (1 μM), a selective IP_3R inhibitor ($P = 0.3$; Fig. 5 *A–C*). Importantly, neither GF109203X nor Xestospongin C

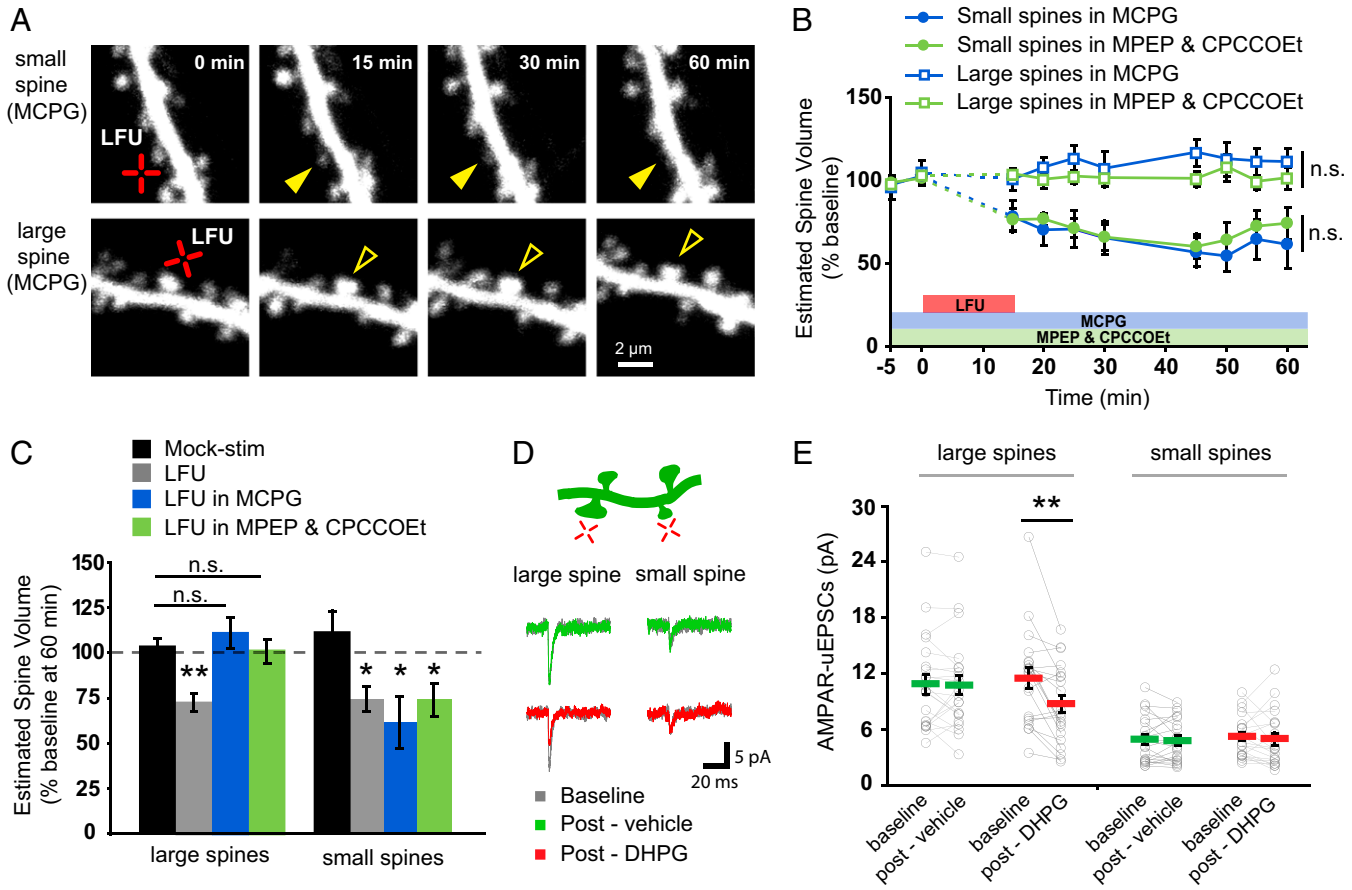

Fig. 4. Activation of group I mGluRs is required for activity-dependent shrinkage of large spines. (*A*) Small (*Upper*) and large (*Lower*) spines were stimulated with LFU in the presence of MCPG (mGluR inhibitor). (*B*) LFU-induced shrinkage of large spines was blocked in the presence of MCPG (open blue squares; $n = 9$ spines, 9 cells) or MPEP and CPCCOEt (open green squares; $n = 14$ spines, 14 cells), whereas small spine shrinkage was unaffected by MCPG (blue circles; $n = 9$ spines, 9 cells) or MPEP and CPCCOEt (green circles; $n = 8$ spines, 8 cells). (*C*) MCPG (blue bar; $P = 0.41$) or MPEP and CPCCOEt (green bar; $P = 0.81$) blocked LFU-induced large spine shrinkage (gray bar; data from Fig. 2) compared with mock-stimulated spines (black bar) at 60 min after LFU. In contrast, the LFU-induced decrease in size of small spines (gray bar; data from Fig. 2) was unaffected by MCPG (blue bar) or MPEP and CPCCOEt (green bar). (*D*) Representative AMPAR-uEPSC traces (8–10 trials at 0.2 Hz) from neighboring large and small spines before (gray) and 5 min after vehicle (green) or DHPG (red) treatment. (*E*) DHPG treatment (red bars) decreased the amplitude of AMPAR-uEPSCs from large spines ($n = 21$ spines, 21 cells) but not from small spines ($P = 0.58$; $n = 21$ spines). Vehicle treatment (green bars) did not affect the AMPAR-uEPSC amplitude from large ($P = 0.86$; $n = 22$ spines, 20 cells) or small ($P = 0.69$; $n = 22$ spines) spines. Open circles represent individual spines; horizontal bars represent the group mean. $^*P < 0.05$; $^{**}P < 0.01$. Error bars are SEM; n.s., not significant.

affected the volume of unstimulated neighboring spines (Fig. 5 *B* and *C*). Together, our data strongly support an important role for calcium release from IP_3R-dependent intracellular stores in activity-dependent shrinkage of large spines.

Discussion

Considerable physiological and biochemical evidence supports LTD as a key cellular mechanism that underlies synaptic weakening during adaptive plasticity (30, 31). LTD has been associated with various forms of structural plasticity in neurons, including increased turnover of presynaptic boutons (32), reduced contact between presynaptic boutons and dendritic spines (33), and spine shrinkage and retraction (17–20). In each of these cases, LFS was implemented using local electrical stimulation and therefore led to changes in populations of spines or synapses. Because our experiments used low-frequency glutamate uncaging at individual dendritic spines, we were successfully able to address the input- and synapse-specificity of spine shrinkage. Our study demonstrates that activity-dependent synaptic weakening and spine shrinkage can occur at individual dendritic spines via an input- and synapse-specific mechanism. Such a mechanism would be critically important for the selective weakening of individual synapses during experience-dependent neural circuit refinement.

We rarely observed that our uncaging stimulus led to complete spine elimination. However, total elimination of established spines in vivo is not infrequent; and this rate is increased in response to experience-dependent plasticity (6, 8), suggesting that activity-dependent mechanisms drive total spine elimination in vivo. Why then do we not observe more cases of LFU-induced spine elimination? One possibility is that activity-dependent spine elimination may occur over longer periods of time (several hours to days). Another possibility could be that complete spine elimination is not exclusively driven by glutamatergic signaling. Because we used glutamate uncaging rather than synaptic stimulation, it is possible that some key presynaptic cofactor is lacking. Alternatively, complete spine loss may not occur via synapse-specific mechanisms; instead, local synaptic competition between spines could drive spine elimination (34).

Our experiments define a critical role for group I mGluR signaling in the regulation of activity-dependent structural plasticity of large, presumably mature spines. Why might large spines require mGluRs in addition to NMDARs? Several studies have identified cofilin, a calcium-dependent F-actin-severing protein, as a critical downstream mediator of NMDARs promoting spine shrinkage and loss in response to LTD (18, 35). Because functional NMDAR numbers are relatively constant between spines (36), larger spines have lower densities of NMDARs. It is therefore plausible to pro-

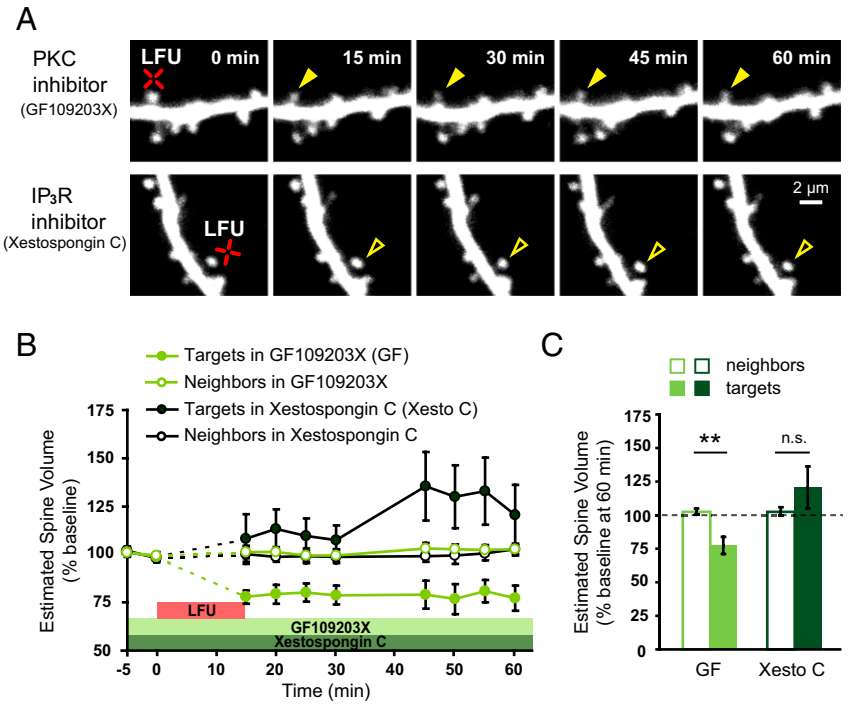

Fig. 5. Activity-dependent shrinkage of large spines requires activation of IP_3R but not PKC. (*A*) The presence of the PKC inhibitor GF109203X did not interfere with LFU-induced large spine shrinkage (*Upper*, yellow arrowheads); in contrast, the IP_3R inhibitor Xestospongin C blocked LFU-induced shrinkage of a large spine (*Lower*, open yellow arrowheads). (*B*) In the presence of GF109203X, LFU persistently shrank large spines (light green circles; n = 12 spines, 12 cells), whereas Xestospongin C blocked LFU-induced large spine shrinkage (dark green circles; n = 12 spines, 12 cells). No change in size was observed for unstimulated neighboring spines in GF109203X (open light green circles; n = 80 spines) or Xestospongin C (open dark green circles; n = 88 spines). (*C*) Inhibition of PKC with GF109203X did not block LFU-induced shrinkage of large spines (light green bar) relative to unstimulated neighbors (open light green bar). In contrast, inhibition of IP_3Rs with Xestospongin C blocked LFU-induced shrinkage of large spines (dark green bar) relative to neighboring spines (open dark green bar; $P = 0.3$). $^{**}P < 0.01$. Error bars are SEM; n.s., not significant.

pose that large spines require contributions of both NMDAR- and group I mGluR-dependent mechanisms to reach a critical "threshold" level of calcium required to support activity-dependent spine shrinkage. Indeed, we define a downstream signaling pathway involving IP_3Rs, which initiate Ca^{2+} release from intracellular stores, in LFU-induced large spine shrinkage.

We show that large spines have higher group I mGluR activity than small spines. What might form the basis for this enhanced mGluR signaling in large spines? One possibility could be that there is a higher concentration of mGluRs in large spines, leading to enhanced signaling. However, despite numerous studies at the ultrastructural level (37–39), differential localization of mGluRs between large and small spines has not been reported. Alternatively, the concentration of mGluRs could be the same between large and small spines, but small spines may lack key downstream signaling molecules that mediate mGluR-dependent synaptic plasticity.

We observed that global stimulation of mGluRs by DHPG led to synaptic weakening at large spines. However, LFU-induced shrinkage of large spines required both mGluR and NMDAR activation. This could suggest that DHPG-induced synaptic weakening is not accompanied by shrinkage of large spines, or that NMDARs are specifically required for the structural, but not the functional depression at large spines. Alternatively, because our LFU stimulation was synapse-specific and less prolonged than bath application of DHPG, and thus likely to have activated a more physiological number of mGluRs, LFU-induced mGluR activity could be insufficient to induce spine shrinkage and synaptic weakening in the absence of NMDAR activation at large spines.

Do mGluRs contribute to experience-dependent structural plasticity of large dendritic spines in vivo? Several studies demonstrate key roles for mGluRs in regulating experience-dependent circuit plasticity in response to visual experience (40, 41), fear conditioning (42), and somatosensory experience (9, 43). Moreover, recent studies of mGluR-dependent synaptic plasticity have led to the discovery of novel cellular and molecular mechanisms with implications for diseases such as Fragile X syndrome and Alzheimer's disease (26, 44, 45). The role of abnormal spine plasticity in driving these phenotypes awaits future in vivo imaging experiments of dendritic spines under these paradigms.

Materials and Methods

Preparation and Transfection of Organotypic Slice Cultures. Organotypic hippocampal slice cultures were prepared from P6-P7 Sprague-Dawley rats, as previously described (46). Genes were delivered 2–3 d before imaging using biolistic gene transfer (180 psi), as previously described (47), except that 20 μg of EGFP (Clontech) was coated onto 6–8 mg of gold particles.

Time-Lapse Two-Photon Imaging. EGFP-transfected CA1 pyramidal neurons [14–18 d in vitro (DIV)] at depths of 20–50 μm were imaged using a custom two-photon microscope with a pulsed Ti::sapphire laser (Mai Tai, Spectra Physics) tuned to 930 nm (0.5–1.5 mW at the sample). The microscope and data acquisition were controlled with ScanImage (48). For each neuron, image stacks (512 × 512 pixels; 0.02 μm per pixel) with 1-μm z-steps were collected from one segment of secondary or tertiary basal dendrites 40–80 μm from the soma. Slices were imaged at 5- to 6-min intervals at 30 °C in recirculating artificial cerebrospinal fluid (ACSF; in mM: 127 NaCl, 25 $NaHCO_3$, 1.2 NaH_2PO_4, 2.5 KCl, 25 D-glucose, aerated with 95%O_2/5%CO_2, ~310 mOsm, pH 7.2). All images shown are maximum projections of 3D image stacks after applying a median filter (3 × 3) to the raw image data.

LFU Stimulus. Uncaging of MNI-glutamate was achieved as previously described (49). In brief, the LFU stimulus consisted of 90 pulses (720 nm; 6–8 mW at the sample) of 1-ms duration delivered at 0.1 Hz by parking the beam at a point ~0.5 μm from the center of the spine head. Imaging-only experiments to assess spine shrinkage were carried out at 30 °C in ACSF containing (in mM): 0.3 Ca^{2+}, 0 Mg^{2+}, 2.5 MNI-glutamate, and 0.001 TTX. Electrophysiological experiments to assess single-spine LTD were carried out at 25 °C in ACSF containing (in mM): 0.3 Ca^{2+}, 1 Mg^{2+}, 2.5 MNI-glutamate, and 0.001 TTX. The mock stimulus was identical in parameters to the LFU stimulus, except carried out in the absence of MNI-glutamate. One target spine per cell was targeted with LFU or mock stimulation.

Image Analysis. Estimated spine volume was measured from background-subtracted green fluorescence using the integrated pixel intensity of a boxed region surrounding the spine head, as previously described (50). Relative spine volume was determined by dividing the estimated volume of an individual spine by the mean estimated volume of all spines on the same dendritic segment. One dendritic region of interest was analyzed per cell,

including the target spine and all clearly visible neighboring spines that were well isolated from each other (average of six neighboring spines per cell).

Electrophysiology. Whole-cell recordings (electrode resistances 5–7 MΩ; series resistances 20–40 MΩ) were performed at 14–18 DIV on visually identified CA1 pyramidal neurons within 40 μm of the slice surface. uEPSCs were recorded at 25 °C in ACSF containing 2.5 mM MNI-glutamate and 1 μM TTX. Uncaging test pulses (1-ms duration, 10–12 mW at the sample) at individual spines (40–80 μm from the soma on secondary or tertiary basal dendrites) elicited an average response of ~8 pA at the soma.

For electrophysiological LTD and group I mGluR activation experiments, CA1 neurons were patched in voltage-clamp configuration (V_{hold} = −65 mV) using cesium-based internal solution (in mM: 135 Cs-methanesulfonate, 10 Hepes, 10 Na_2 phosphocreatine, 4 $MgCl_2$, 4 Na_2-ATP, 0.4 Na-GTP, 3 Na L-ascorbate, 0.2 Alexa 488, and ~300 mOsm, ~pH 7.25) in ACSF at 25 °C. For single-spine LTD experiments, uEPSCs were acquired in ACSF (0.3 mM Ca^{2+}, 1 mM Mg^{2+}) from one target and one or two neighboring spines. After a short baseline, LTD was induced at the target spine by pairing the LFU stimulus with postsynaptic depolarization to 0 mV (200-ms step starting 100 ms before uncaging pulse). For group I mGluR activation experiments, 10 μM CPP was added to the ACSF (2 mM Ca^{2+}, 1 mM Mg^{2+}) and uEPSCs were acquired from two spines (one large and one small, 3–10 μm apart). After a short baseline, mGluR-LTD was induced by a 5-min wash-in of 100 μM DHPG. uEPSC amplitudes from individual spines were quantified as the average (8–10 test pulses at 0.2 Hz) from a 2-ms window centered on the maximum current amplitude within 50 ms after pulse delivery.

To monitor spiking properties and excitatory postsynaptic potential (EPSP) frequency, whole-cell properties were recorded in current-clamp mode using potassium-based internal solution (in mM: 136 $KMeSO_3$, 10 Hepes, 17.5 KCl, 9 NaCl, 1 $MgCl_2$, 4 Na_2-ATP, 0.4 Na-GTP, 0.2 EGTA, and ~300 mOsm, ~pH 7.3) at 25 °C in ACSF containing 2 mM Ca^{2+} and 1 mM Mg^{2+}. To examine spiking properties, the minimum amount of current required to elicit action potential firing was measured by injecting depolarizing current steps. Action potentials evoked by the minimum step current injections (150–200 pA, 0.6 s) were recorded before and after DHPG application (4 μM, 5 min) from neurons preincubated with mGluR inhibitor(s) or vehicle(s). EPSP frequency was measured before and after phorbol 12-myristate 13-acetate (PMA) application (1 nM, 3 min) from neurons preincubated with GF109203X or vehicle.

Pharmacology. Stocks were prepared at 1,000× (or greater) by dissolving TTX (Calbiochem), CPP (Sigma), DHPG, and MPEP in water; CPCCOEt, GF109203X, PMA, and Xestospongin C in DMSO; and MCPG in 1 N NaOH. All drugs were from Tocris unless otherwise noted. Vehicle controls were matched in identity and volume to that in which the drug was dissolved.

Statistics. Data from a minimum of 6 independent culture preparations (average of 10) were used for each experimental comparison. All statistics were calculated across cells. Error bars represent SEM, and significance was set at $P = 0.05$ (Student's two-tailed t test).

ACKNOWLEDGMENTS. We thank Lauren Boudewyn and Julie Heiner for help with experiments; Hwai-Jong Cheng, Laura Borodinsky, and Johannes Hell for valuable discussion; and Elva Diaz, Hyung-Bae Kwon, Hugo Vega-Ramirez, Vu Trinh, and members of the Zito laboratory for critical reading of the manuscript. This work was supported by National Institutes of Health Grant NS062736 and a Burroughs Wellcome Career Award in the Biomedical Sciences.

1. Holtmaat A, Svoboda K (2009) Experience-dependent structural synaptic plasticity in the mammalian brain. *Nat Rev Neurosci* 10(9):647–658.
2. Kasai H, Fukuda M, Watanabe S, Hayashi-Takagi A, Noguchi J (2010) Structural dynamics of dendritic spines in memory and cognition. *Trends Neurosci* 33(3):121–129.
3. Holtmaat AJ, et al. (2005) Transient and persistent dendritic spines in the neocortex in vivo. *Neuron* 45(2):279–291.
4. Zuo Y, Lin A, Chang P, Gan WB (2005) Development of long-term dendritic spine stability in diverse regions of cerebral cortex. *Neuron* 46(2):181–189.
5. Wise SP, Fleshman JW, Jr., Jones EG (1979) Maturation of pyramidal cell form in relation to developing afferent and efferent connections of rat somatic sensory cortex. *Neuroscience* 4(9):1275–1297.
6. Holtmaat A, Wilbrecht L, Knott GW, Welker E, Svoboda K (2006) Experience-dependent and cell-type-specific spine growth in the neocortex. *Nature* 441(7096):979–983.
7. Xu T, et al. (2009) Rapid formation and selective stabilization of synapses for enduring motor memories. *Nature* 462(7275):915–919.
8. Yang G, Pan F, Gan WB (2009) Stably maintained dendritic spines are associated with lifelong memories. *Nature* 462(7275):920–924.
9. Tschida KA, Mooney R (2012) Deafening drives cell-type-specific changes to dendritic spines in a sensorimotor nucleus important to learned vocalizations. *Neuron* 73(5):1028–1039.
10. Harris KM, Jensen FE, Tsao B (1992) Three-dimensional structure of dendritic spines and synapses in rat hippocampus (CA1) at postnatal day 15 and adult ages: Implications for the maturation of synaptic physiology and long-term potentiation. *J Neurosci* 12(7):2685–2705.
11. Harris KM, Stevens JK (1989) Dendritic spines of CA 1 pyramidal cells in the rat hippocampus: Serial electron microscopy with reference to their biophysical characteristics. *J Neurosci* 9(8):2982–2997.
12. Trachtenberg JT, et al. (2002) Long-term in vivo imaging of experience-dependent synaptic plasticity in adult cortex. *Nature* 420(6917):788–794.
13. Yasumatsu N, Matsuzaki M, Miyazaki T, Noguchi J, Kasai H (2008) Principles of long-term dynamics of dendritic spines. *J Neurosci* 28(50):13592–13608.
14. Kasai H, Matsuzaki M, Noguchi J, Yasumatsu N, Nakahara H (2003) Structure-stability-function relationships of dendritic spines. *Trends Neurosci* 26(7):360–368.
15. Zuo Y, Yang G, Kwon E, Gan WB (2005) Long-term sensory deprivation prevents dendritic spine loss in primary somatosensory cortex. *Nature* 436(7048):261–265.
16. Dudek SM, Bear MF (1992) Homosynaptic long-term depression in area CA1 of hippocampus and effects of N-methyl-D-aspartate receptor blockade. *Proc Natl Acad Sci USA* 89(10):4363–4367.
17. Nägerl UV, Eberhorn N, Cambridge SB, Bonhoeffer T (2004) Bidirectional activity-dependent morphological plasticity in hippocampal neurons. *Neuron* 44(5):759–767.
18. Zhou Q, Homma KJ, Poo MM (2004) Shrinkage of dendritic spines associated with long-term depression of hippocampal synapses. *Neuron* 44(5):749–757.
19. Okamoto K, Nagai T, Miyawaki A, Hayashi Y (2004) Rapid and persistent modulation of actin dynamics regulates postsynaptic reorganization underlying bidirectional plasticity. *Nat Neurosci* 7(10):1104–1112.
20. Wang XB, Yang Y, Zhou Q (2007) Independent expression of synaptic and morphological plasticity associated with long-term depression. *J Neurosci* 27(45):12419–12429.
21. Matsuzaki M, Honkura N, Ellis-Davies GC, Kasai H (2004) Structural basis of long-term potentiation in single dendritic spines. *Nature* 429(6993):761–766.
22. Matsuzaki M, et al. (2001) Dendritic spine geometry is critical for AMPA receptor expression in hippocampal CA1 pyramidal neurons. *Nat Neurosci* 4(11):1086–1092.
23. Bienenstock EL, Cooper LN, Munro PW (1982) Theory for the development of neuron selectivity: Orientation specificity and binocular interaction in visual cortex. *J Neurosci* 2(1):32–48.
24. Vanderklish PW, Edelman GM (2002) Dendritic spines elongate after stimulation of group 1 metabotropic glutamate receptors in cultured hippocampal neurons. *Proc Natl Acad Sci USA* 99(3):1639–1644.
25. Holbro N, Grunditz A, Oertner TG (2009) Differential distribution of endoplasmic reticulum controls metabotropic signaling and plasticity at hippocampal synapses. *Proc Natl Acad Sci USA* 106(35):15055–15060.
26. Michalon A, et al. (2012) Chronic pharmacological mGlu5 inhibition corrects fragile X in adult mice. *Neuron* 74(1):49–56.
27. Lüscher C, Huber KM (2010) Group 1 mGluR-dependent synaptic long-term depression: Mechanisms and implications for circuitry and disease. *Neuron* 65(4):445–459.
28. Di Paolo G, De Camilli P (2006) Phosphoinositides in cell regulation and membrane dynamics. *Nature* 443(7112):651–657.
29. Calabrese B, Halpain S (2005) Essential role for the PKC target MARCKS in maintaining dendritic spine morphology. *Neuron* 48(1):77–90.
30. Malenka RC, Bear MF (2004) LTP and LTD: An embarrassment of riches. *Neuron* 44(1):5–21.
31. Feldman DE (2009) Synaptic mechanisms for plasticity in neocortex. *Annu Rev Neurosci* 32:33–55.
32. Becker N, Wierenga CJ, Fonseca R, Bonhoeffer T, Nägerl UV (2008) LTD induction causes morphological changes of presynaptic boutons and reduces their contacts with spines. *Neuron* 60(4):590–597.
33. Bastrikova N, Gardner GA, Reece JM, Jeromin A, Dudek SM (2008) Synapse elimination accompanies functional plasticity in hippocampal neurons. *Proc Natl Acad Sci USA* 105(8):3123–3127.
34. Lo YJ, Poo MM (1991) Activity-dependent synaptic competition in vitro: Heterosynaptic suppression of developing synapses. *Science* 254(5034):1019–1022.
35. Pontrello CG, et al. (2012) Cofilin under control of β-arrestin-2 in NMDA-dependent dendritic spine plasticity, long-term depression (LTD), and learning. *Proc Natl Acad Sci USA* 109(7):E442–E451.
36. Sobczyk A, Scheuss V, Svoboda K (2005) NMDA receptor subunit-dependent [Ca2+] signaling in individual hippocampal dendritic spines. *J Neurosci* 25(26):6037–6046.
37. Lujan R, Nusser Z, Roberts JD, Shigemoto R, Somogyi P (1996) Perisynaptic location of metabotropic glutamate receptors mGluR1 and mGluR5 on dendrites and dendritic spines in the rat hippocampus. *Eur J Neurosci* 8(7):1488–1500.
38. Baude A, et al. (1993) The metabotropic glutamate receptor (mGluR1 alpha) is concentrated at perisynaptic membrane of neuronal subpopulations as detected by immunogold reaction. *Neuron* 11(4):771–787.
39. López-Bendito G, Shigemoto R, Fairén A, Luján R (2002) Differential distribution of group I metabotropic glutamate receptors during rat cortical development. *Cereb Cortex* 12(6):625–638.
40. Van Keuren-Jensen K, Cline HT (2006) Visual experience regulates metabotropic glutamate receptor-mediated plasticity of AMPA receptor synaptic transmission by homer1a induction. *J Neurosci* 26(29):7575–7580.
41. Matta JA, Ashby MC, Sanz-Clemente A, Roche KW, Isaac JT (2011) mGluR5 and NMDA receptors drive the experience- and activity-dependent NMDA receptor NR2B to NR2A subunit switch. *Neuron* 70(2):339–351.
42. Clem RL, Huganir RL (2010) Calcium-permeable AMPA receptor dynamics mediate fear memory erasure. *Science* 330(6007):1108–1112.

43. Clem RL, Celikel T, Barth AL (2008) Ongoing in vivo experience triggers synaptic metaplasticity in the neocortex. *Science* 319(5859):101–104.
44. Ronesi JA, et al. (2012) Disrupted Homer scaffolds mediate abnormal mGluR5 function in a mouse model of fragile X syndrome. *Nat Neurosci* 15(3):431–440, S431.
45. Hsieh H, et al. (2006) AMPAR removal underlies Abeta-induced synaptic depression and dendritic spine loss. *Neuron* 52(5):831–843.
46. Stoppini L, Buchs PA, Muller D (1991) A simple method for organotypic cultures of nervous tissue. *J Neurosci Methods* 37(2):173–182.
47. Woods G, Zito K (2008) Preparation of gene gun bullets and biolistic transfection of neurons in slice culture. *J Vis Exp* 12):12.
48. Pologruto TA, Sabatini BL, Svoboda K (2003) ScanImage: Flexible software for operating laser scanning microscopes. *Biomed Eng Online* 2:13.
49. Zito K, Scheuss V, Knott G, Hill T, Svoboda K (2009) Rapid functional maturation of nascent dendritic spines. *Neuron* 61(2):247–258.
50. Woods GF, Oh WC, Boudewyn LC, Mikula SK, Zito K (2011) Loss of PSD-95 enrichment is not a prerequisite for spine retraction. *J Neurosci* 31(34):12129–12138.

Supporting Information

Oh et al. 10.1073/pnas.1214705110

SI Materials and Methods

Design of Low-Frequency Glutamate Uncaging Stimulus. To design a glutamate uncaging stimulus that would mimic a conventional low-frequency synaptic stimulation (900 pulses at 1 Hz) (1), which induces long-term depression (LTD) of a population of spines proximal to the stimulating electrode (2), the stimulation rate was reduced 10-fold [low-frequency glutamate uncaging (LFU); 90 pulses at 0.1 Hz] to account for the average release probability of glutamate at Schaffer collateral synapses, which is less than 0.2 (3). In addition, as suggested by the Bienenstock, Cooper, and Munro (BCM) model (4, 5), which predicts that a modest but prolonged rise in postsynaptic calcium induces LTD (6, 7), lower extracellular Ca^{2+} concentration (0.3 mM) was used. Last, to remove the Mg^{2+} blockade of the NMDA receptor (NMDAR) during whole-cell recordings, each uncaging pulse was paired with a 200-ms depolarization to 0 mV, and imaging-only experiments were carried out in nominal Mg^{2+}.

1. Dudek SM, Bear MF (1992) Homosynaptic long-term depression in area CA1 of hippocampus and effects of N-methyl-D-aspartate receptor blockade. *Proc Natl Acad Sci USA* 89(10):4363–4367.
2. Zhou Q, Homma KJ, Poo MM (2004) Shrinkage of dendritic spines associated with long-term depression of hippocampal synapses. *Neuron* 44(5):749–757.
3. Branco T, Staras K (2009) The probability of neurotransmitter release: Variability and feedback control at single synapses. *Nat Rev Neurosci* 10(5):373–383.
4. Bienenstock EL, Cooper LN, Munro PW (1982) Theory for the development of neuron selectivity: Orientation specificity and binocular interaction in visual cortex. *J Neurosci* 2(1):32–48.
5. Cooper LN, Bear MF (2012) The BCM theory of synapse modification at 30: Interaction of theory with experiment. *Nat Rev Neurosci* 13(11):798–810.
6. Bear MF (1995) Mechanism for a sliding synaptic modification threshold. *Neuron* 15(1):1–4.
7. Lüscher C, Malenka RC (2012) NMDA receptor-dependent long-term potentiation and long-term depression (LTP/LTD). *Cold Spring Harb Perspect Biol* 4(6):4.

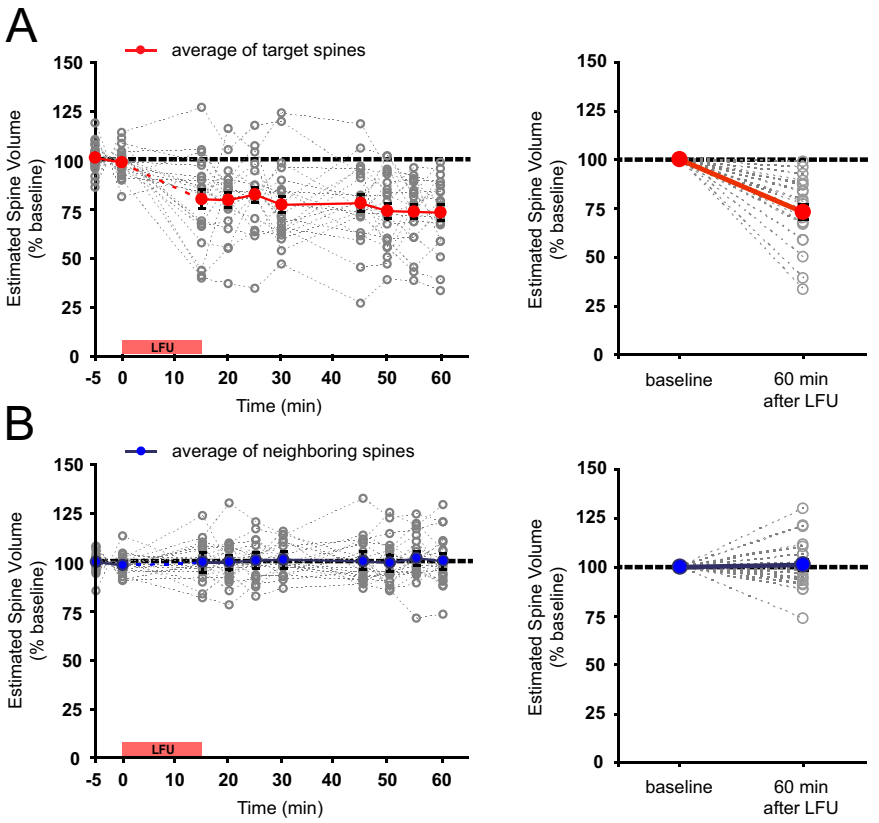

Fig. S1. LFU-induced spine shrinkage is synapse specific and long lasting. (*A*) LFU persistently decreased the volume of target spines. Open gray circles represent individual target spines ($n = 21$ spines, 21 cells), and red circles represent the group mean ($P < 0.01$ relative to baseline at all post-LFU time points). (*Right*) Final post-LFU time point relative to baseline (mean of two baseline time points). (*B*) In contrast, the size of neighboring spines did not change over time. Open gray circles represent the average size of neighboring spines of individual targets ($n = 132$ neighboring spines, 21 cells; average of 6.3 ± 0.3 neighboring spines per target) and blue circles represent the group mean. (*Right*) Final post-LFU time point relative to baseline. Error bars are SEM.

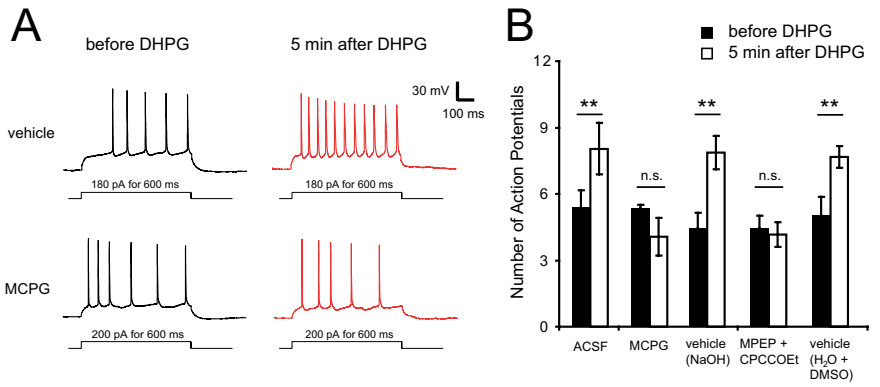

Fig. S2. Metabotropic glutamate receptor (mGluR) inhibitors block DHPG activation of mGluRs. (*A*) Example traces showing voltage responses to step current injections of 180 pA or 200 pA for 0.6 s. Black traces are baseline responses in CA1 of rat hippocampal slices preincubated with vehicle (NaOH) or mGluR inhibitor (MCPG) before the onset of 4 μM DHPG perfusion. Red traces are responses to the same current injection after a 5-min DHPG application. (*B*) Step current injections (150–200 pA, just above threshold for action potential firing) in vehicle controls (water for DHPG; NaOH for MCPG; water + DMSO for MPEP + CPCCOEt) elicited increased action potential firing in response to DHPG. In contrast, 10-min preincubation with MCPG (0.25 mM) or MPEP (15 μM) + CPCCOEt (45 μM) rapidly and completely blocked DHPG activation of group I mGluRs (DHPG vehicle, five cells; MCPG, five cells; MCPG vehicle, five cells; MPEP + CPCCOEt, six cells; MPEP + CPCCOEt vehicles, five cells). $^{**}P < 0.01$. Error bars are SEM; n.s., not significant.

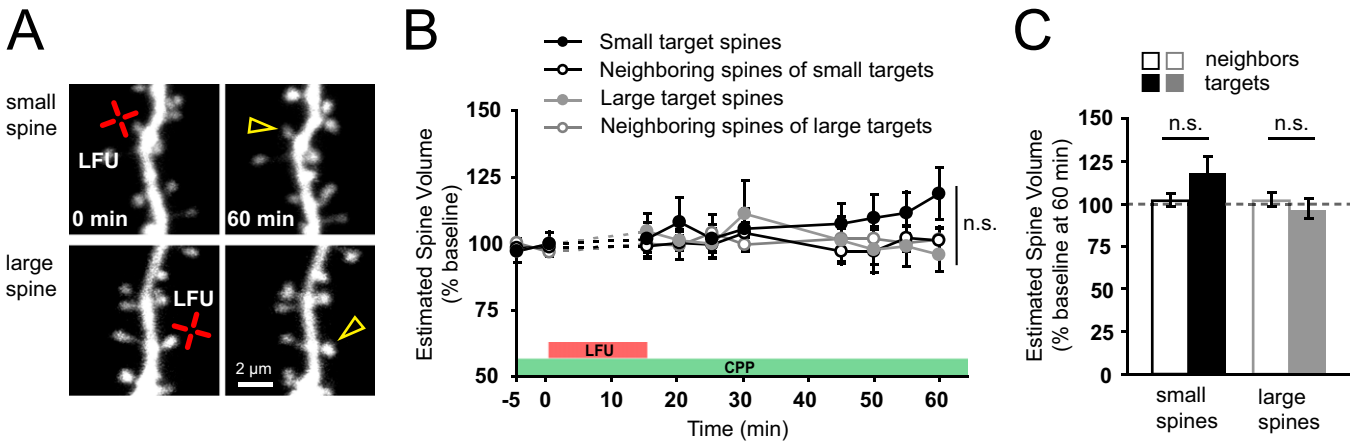

Fig. S3. NMDAR blockade completely abolishes shrinkage of both small and large spines. (*A*) Images of dendritic spines from EGFP-transfected CA1 pyramidal neurons at 14–18 DIV. Both small and large spines were targeted and stimulated with LFU (red cross) in the presence of CPP (10 μM), and the effect of LFU on spine volume was examined for up to 60 min (open yellow arrowheads). (*B*) In the presence of CPP, no LFU-induced decrease in spine size was observed for the stimulated small (filled black circles; $n = 10$ spines, 10 cells) or large (filled gray circles; $n = 11$ spines, 11 cells) spines over baseline or relative to unstimulated neighboring spines of small (open black circles; $n = 71$ spines, 10 cells) and large (open gray circles; $n = 72$ spines, 11 cells) target spines. (*C*) 60 min after LFU, in the presence of CPP, the volume of small target spines (solid black bar) was not significantly different from that of neighboring spines (open black bar; $P = 0.13$). In addition, LFU did not shrink large spines (solid gray bar) compared with neighboring spines (open gray bar; $P = 0.47$). Error bars are SEM; n.s., not significant.

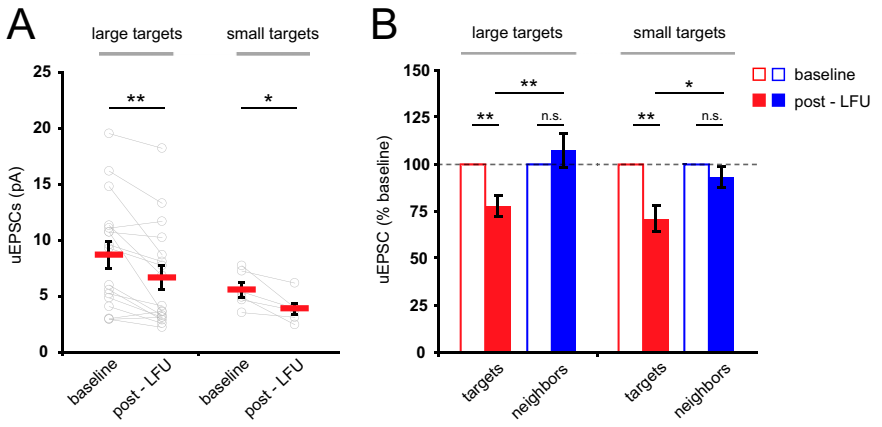

Fig. S4. LFU leads to depression of uEPSCs from both small and large spines. (*A*) LFU decreased the amplitude of uEPSCs from large ($n = 17$ spines, 17 cells) and small ($n = 6$ spines, 6 cells) spines. Open circles represent individual spines and horizontal bars represent the group mean. (*B*) For both large and small target spines, uEPSCs of the targets (red bars) were decreased in response to LFU compared with baseline (open red bars) and also to neighboring spines (blue bars). Neither neighbors of the large targets ($P = 0.42$; $n = 19$ spines, 17 cells) nor neighbors of the small targets ($P = 0.29$; $n = 7$ spines, 6 cells) were depressed compared with baseline (open blue bars). $*P < 0.05$; $**P < 0.01$. Error bars are SEM; n.s., not significant.

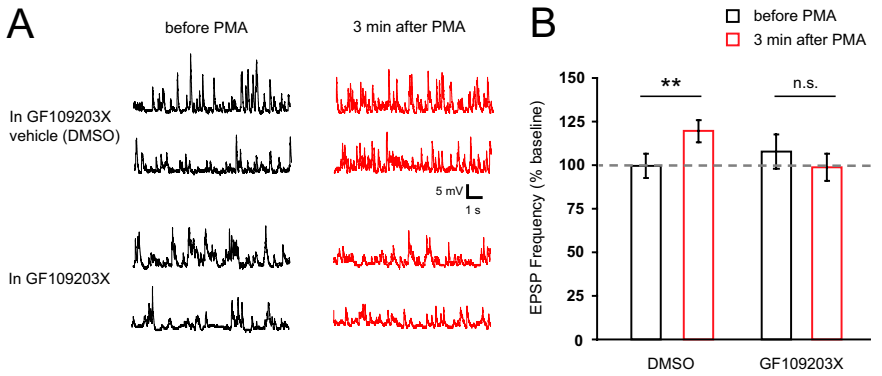

Fig. S5. GF109203X blocks PKC-mediated increase in EPSP frequency. (*A*) Recordings were made from pyramidal neurons in the CA1 region of hippocampal slices at 14–18 DIV. Black and red traces show EPSPs before and after a 3-min PMA application in the presence of vehicle (DMSO) or GF109203X, respectively. (*B*) Brief bath application of a low concentration of PKC activator, PMA (1 nM), significantly increased EPSP frequency in DMSO control ($n = 6$ cells), whereas preincubation with GF109203X (1 μM) for 10 min completely abolished PMA-induced increase in EPSP frequency ($P = 0.43$, $n = 5$ cells). Preincubation of hippocampal slices with DMSO or GF109203X alone for 10 min did not alter EPSP frequency over baseline (DMSO, $P = 0.97$, $n = 6$ cells; GF109203X, $P = 0.48$, $n = 5$ cells). $**P < 0.01$. Error bars are SEM; n.s., not significant.